

Optimal design of a hybrid power generation system based on integrating PEM fuel cell and PEM electrolyzer as a moderator for micro-renewable energy systems

Armin Abdollahipour, Hoseyn Sayyaadi *

Lab of Optimization of Thermal Systems' Installations, Faculty of Mechanical Engineering-Energy Division, K.N. Toosi University of Technology, P.O. Box: 19395-1999, No. 15-19, Pardis St., Mollasadra Ave., Vanak Sq., Tehran, 1999 143344, Iran

ARTICLE INFO

Keywords:

Economic analysis
 Electrochemical
 Optimization
 Pem fuel cell
 Pem electrolyzer
 Power generation

ABSTRACT

Proton exchange membrane fuel cell (PEMFC) and proton exchange membrane electrolyzer cell (PEMEC) are integrated for power generation and reduce power production fluctuations of renewable energy technologies. For this purpose, the three-dimensional model of the PEMFC and PEMEC are numerically simulated. Afterward, the integrated power generation system performance is evaluated in terms of power output, efficiency, and leveled cost of electricity. The performance analysis showed the necessity of multi-objective optimization for the power generation system. In this regard, three scenarios are considered for optimization. In the first case, power output and efficiency, and in the second scenario, power output and leveled cost are considered objective functions. Finally, in the third scenario, the three abovementioned parameters are considered three objective functions. For choosing the final optimal solution, decision-making techniques are employed. Results of decision-making techniques showed that the third scenario was the complete case to optimize the system. Furthermore, the TOPSIS method provided a more favorable final optimal solution with the lowest value for the leveled cost of the system, $0.498 \text{ } \$\text{kWh}^{-1}$, while the efficiency and output power of the power generation system were 0.323 and 1801.87 W m^{-2} , respectively. Considering that the efficiency and cost of the PEMFCs and PEMECs are expected to improve drastically over time, these systems could be a promising option for power generation applications.

1. Introduction

Fuel cells have been regarded as a potential replacement for conventional power generation technologies because of their lower greenhouse gas emissions and high efficiency. The proton exchange membrane fuel cell (PEMFC) is widely used because of low environmental pollution, low operating temperature [1], high efficiency [2], simple structure, quick start-up [3]. The PEMFC uses hydrogen as fuel. Currently, the reforming of hydrocarbons such as methane is used to produce hydrogen, which is a process that pollutes the environment. Water electrolysis is a promising way to produce hydrogen from water at small scales [4]. Among diverse water electrolysis systems, proton exchange membrane electrolyzer cell (PEMEC) has attracted attention due to higher purity and rate of hydrogen production, higher energy efficiency, lower power consumption, more compact system design [5], safety because of non-corrosive and non-hazardous electrolytes, and the

possibility of integration with fuel cells [6].

Clean and sustainable power generation technologies can be a suitable replacement for current coal/oil fuels and their related issues. Renewable energy sources such as solar and wind energy [7], due to their availability and endlessness, are considered as preferred technologies [8]. However, one of the main challenges for these two technologies is the periodic characteristics of the natural resources used by these technologies. Thus the generation of continuous and reliable power is not possible. For solving this issue, intermediate energy sources can be utilized to reduce power production fluctuations. Therefore, when additional power is generated, it is transformed to intermediate energy sources, and this provided energy is utilized when there is a power shortage. One of the intermediate energy sources is hydrogen.

Currently, novel applications of integrated PEMFCs with PEMECs are expanding, and the feasibility evaluation of integrating them seems crucial [9]. Renewable energies can not produce constant power due to

* Corresponding author.

E-mail addresses: abdollahipourarmin@gmail.com (A. Abdollahipour), sayyaadi@kntu.ac.ir, hoseynsayyaadi@gmail.com (H. Sayyaadi).

their fluctuating nature. Hence, to achieve a constant electric output, the power generated by renewable sources can be utilized to generate hydrogen via PEMEC. The generated hydrogen may be stored and used by the PEMFC for a constant and non-fluctuating power generation. Therefore, the main idea of this paper is the production of hydrogen by PEMEC when these renewable energies are sufficient. Then in times of shortage of these energies, the stored hydrogen previously produced by the PEMEC can be used as fuel in the PEMFC. As a result, we will have a hybrid system for oscillating power generation of renewable technologies resulting from integrating the PEMFC and PEMEC.

Solar [10], wind [11], and geothermal [12] energies are three leading technologies for hydrogen production. Touili et al. [13] investigated the production of hydrogen from solar energy in Morocco; for this purpose photovoltaic-electrolyze system was chosen. Results indicated that a considerable potential for hydrogen production from solar energy could be achieved in Morocco. Mostafaeipour et al. [14] evaluated Iran's solar-powered hydrogen production potential. Solar-powered electricity is generated by the photovoltaic system used for producing hydrogen. Solar photovoltaic/PEM water electrolytes evaluated in Sahara regions of Algeria [15]. The effect of weather conditions on hydrogen production was also investigated, and an integrated floating photovoltaic system was developed for electricity generation and hydrogen production.

The floating photovoltaic system generated the electricity and extra electricity used to produce hydrogen in the electrolyzer. During the night or cloudy weather where the solar energy was not available, stored hydrogen was utilized by the fuel cell to produce needed electricity. Ayodele and Munda [16] used wind energy with water electrolysis for hydrogen production. The effects of different parameters on hydrogen production were evaluated, and results showed that wind speed has a considerable influence on the hydrogen production cost. Ishaq et al. [17] investigated the performance of combined wind turbine, water electrolyzer, and pem fuel cells for providing electricity to households. During high wind speeds, the extra electricity utilized by the electrolyzer for hydrogen production which later used by fuel cells when wind speed is low. The overall energy efficiency of the system was found to be 20.2%. Li et al. [18] reviewed the development of hydrogen production by wind power generation. Hydrogen is also produced by combined solar and wind energy [19]. Al-Sharafi et al. [20] investigated power generation and hydrogen production by solar and wind energy systems in Saudi Arabia. The wind turbines and PV array combined with an electrolyzer, fuel cell, batteries, and hydrogen tank. Copuling of electrolyzer with different renewable energy sources, including solar energy, wind energy, geothermal energy, ocean thermal energy conversion system and hydroelectric energy reviewed by Mohammadi and Mehrpooya [8]. They concluded that currently hydroelectric is the most promising renewable source to produce hydrogen. Vaziri Rad et al. [21] investigated an optimal renewable energy system to meet the load of a small village by renewable resources. A hybrid photovoltaics/wind turbine/biogas generator/fuel cell renewable energy system proposed alongside a hydrogen tank, batteries, and a reformer or an electrolyzer, to act as storage system. Wu et al. [22] utilized a wastewater treatment process for hydrogen production and connected it to the PEMFC to form the stand-alone PV/FC/battery hybrid power system and the proposed system was optimized techno-economically. Hosseini Dehshiri [23] investigated the feasibility of hybrid energy systems in Isfahan, Iran. Results indicated that among the hydrogen storage scenarios, the most suitable system was PV-CV-electrolyzer-hydrogen tank-fuel cell. Yilmaz and Kanoglu [24] performed energy and exergy analysis of hydrogen production by geothermal driven PEM water electrolyzer. Analysis results revealed that both energy and exergy efficiencies increase with electrolysis temperature. The economic feasibility of different hydrogen production technologies was investigated by Fan et al. [25]. Results revealed that the leveled cost of hydrogen of coal-to-hydrogen coupled CCS was lower about 20.5–61.0% in comparison with the hydrogen production via the water electrolysis powered by renewable energy. The

scramjet multi-expansion open cooling cycle coupled with a PEM electrolyzer was employed by Seyedmatin et al. [26] for both power and hydrogen extraction.

The main contribution of this study is to investigate the performance of PEMFC and PEMEC when they are integrated, based on critical parameters. Furthermore, this study incorporates an economic approach to couple the power generation and integrated system efficiency with economic aspects of the integrated system. Electrochemical and economic analyzes of the system are of great importance because nowadays, the cost is the most crucial factor in choosing renewable energy systems and technologies. Also, to evaluate the near-reality performance of PEMFC and PEMEC systems, these two systems are simulated numerically and three-dimensionally. Then, their polarization curves are extracted for analytical and economic analysis, and very precise correlations are fitted on them. In addition, multi-objective optimization of the integrated system using the genetic algorithm as a differential factor from former studies clarifies this system's feasibility and attractiveness compared to other hydrogen production technologies. As a result, our research contributes to closing the knowledge gap regarding integrating the PEMFC and PEMEC for power generation. In summary, the novelties of this study are as follows:

- A complete multi-objective optimization: power output density, energy efficiency, and leveled cost of electricity for the integrated system are considered objective functions in three different scenarios. Thus, electrochemical analysis with economic analysis is considered together—the genetic algorithm employed to optimize the hybrid system.
- Methodology of investigation of the integrated system: the investigation method combines numerical simulation and analytical analysis. The PEMFC and the PEMEC were numerically simulated using a 3D model; then, the numerical results were used as inputs for analytical and economic simulation steps.

Therefore, in the present study, the three-dimensional model of the PEMFC and PEMEC are numerically simulated. The integration of the PEMFC and PEMEC for power generation is then investigated, and the intended system is thermo-economically optimized with multi-objective optimization employing the genetic algorithm. In the 2nd section, first, the structure of the integrated PEMFC and PEMEC system for power generation is introduced. Then in the 3rd section, the PEMFC and PEMEC are simulated numerically, and their governing equations are expressed. In the 4th section, the numerical simulation models created for the PEMFC and PEMEC are validated with the experimental results of previous studies. Moreover, the performance of the power generation system and its optimization are expressed. Finally, suggestions for future work are made.

2. System description

Since the required voltage of the PEMEC is consistently higher than that of PEMFC; hence, the TREC structure cannot be used for power generation in a standalone installation. Therefore, another structure for power generation is proposed by coupling these two systems. Due to the periodic characteristics of renewable energies such as wind and solar energy, generating reliable power with photovoltaic modules or wind turbines is challenging. To solve this problem, intermediate power generation systems can be used to reduce power fluctuations. Therefore, when renewable energy technologies generate excess power, this power can be transferred to intermediate power generation systems. In the event of power shortages, these systems can be used to supply energy. Hydrogen can be used as a source of intermediate energy. Fig. 1 shows the schematic of the proposed system for power generation, including the PEMEC and the PEMFC. As mentioned, if there is additional power, hydrogen can be produced as an intermediate energy source by the PEMEC. The hydrogen is then consumed by the PEMFC in a power

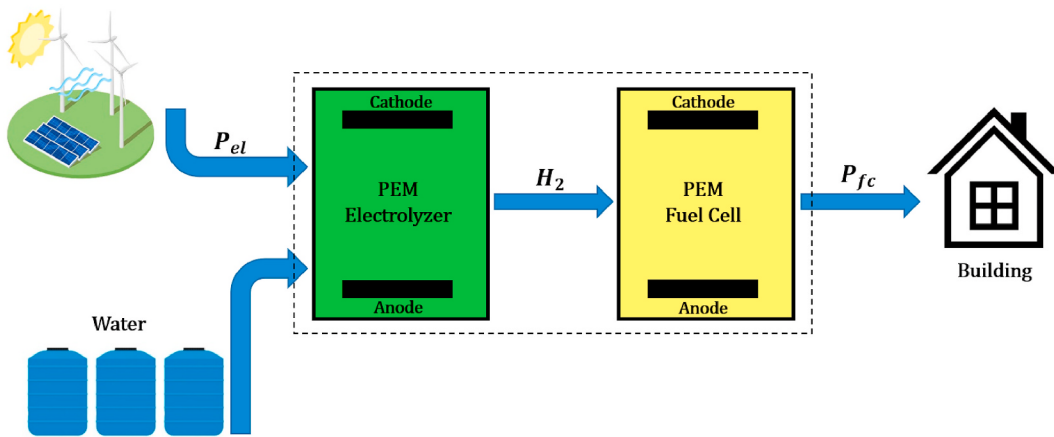


Fig. 1. Schematic of coupling the PEMFC and PEMEC system for power generation.

shortage and generates electrical energy. It is worth noting that the idea of this system is as a support system to withstand power fluctuations and excessive demand conditions in the primary energy systems (e.g., wind turbines and photovoltaic panels). Therefore, the study of the proposed coupling system focuses on the production of electrical energy by the PEMFC. The PEMEC supplies its fuel, and the primary energy sources also supply the power of the PEMEC itself.

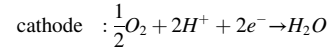
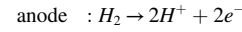
3. Modeling

Various models have been proposed for analyzing the PEMFC and PEMEC, including experimental, analytical models [27], and numerical simulations [28,29]. In this section, first, the PEMFC and PEMEC are numerically simulated, and their governing equations are expressed. Then, the integrated system is analytically investigated in terms of economic aspects.

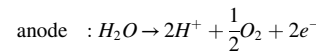
3.1. Numerical model

The same 3D geometric structure is used to model the PEM fuel cell (PEMFC) and the PEM electrolyzer cell (PEMEC). The basic schematic of the structure is shown in Fig. 2. The computational domain consists of anode and cathode flow channels, gas diffusion layers (GDLs), catalyst layers on both anode and cathode sides, and membrane layer. For the fuel cell, on the anode side, hydrogen is injected into the gas channel and directed to the catalyst layer through the gas diffusion layer, a porous medium. The catalyst layer is a very thin layer obtained by placing platinum on the gas diffusion layer. This layer is also porous. Hydrogen

is decomposed by chemical reactions into electrons and protons in the catalyst layer. Next to the catalyst layer is a polymer membrane. Membrane resists the movement of electrons while allowing hydrogen ions to pass through. Finally, electrons flow through the external circuit to the cathode while protons pass through the membrane. Air or oxygen gas is injected into the cathode gas channel and reaches the catalyst through the cathode gas diffusion layer. At the catalyst layer of the cathode side, oxygen and hydrogen ions subsequently react, along with electrons transferred from the external circuit to form a byproduct, water. Contrary, for the PEM electrolyzer, water is decomposed into oxygen, proton, and electrons on the anode side. The migrated proton through the membrane with electrons forms hydrogen on the cathode side. The anode and cathode side reactions for the PEMFC are as follows:



and for PEMEC:



The following assumptions have been used to simulate the PEMFC and PEMEC [30]:

- Steady-state operation for the PEMFC and PEMEC

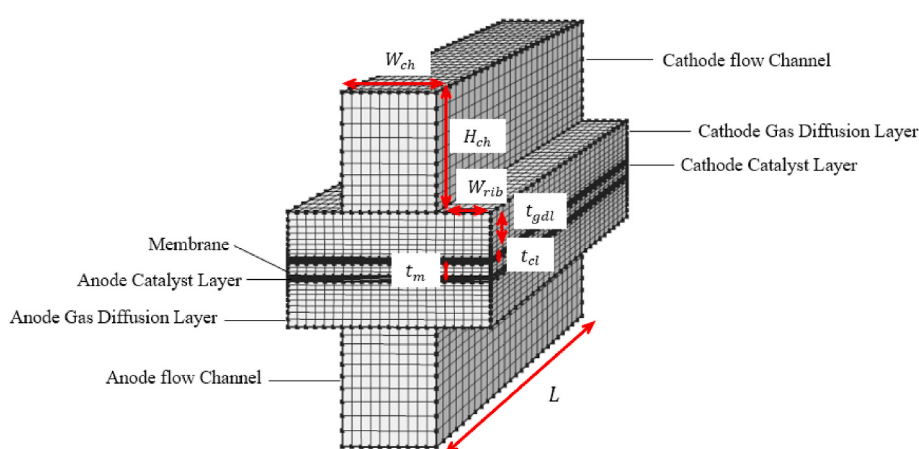


Fig. 2. Three-dimensional computational domain of PEMFC and PEMEC model.

- Ideal gas consideration for reactions, hydrogen, and air
- Laminar gas flow through the channels
- Homogeneous porous media in the gas diffusion layers, catalyst layers, and membranes
- Constant thermal and electrical conductivity of the materials

3.1.1. Governing equations

The governing equations include conservation of mass and momentum, energy, species transport equation, electric charge conservation. The conservation of mass equation is written as follows [31,32]:

$$\nabla \cdot (\varepsilon \rho \vec{u}) = S_m \quad (1)$$

where ε porosity, ρ is the density of the mixture, u is velocity, and is the source term of continuity equation and equal to zero for PEMFC and PEMEC. The momentum conservation equation is as follows [31,32]:

$$\rho \left[(\vec{u} \cdot \nabla) \frac{\vec{u}}{\varepsilon} \right] = -\nabla p + \nabla \cdot \left[\frac{1}{\varepsilon} (\mu (\nabla \vec{u} + (\nabla \vec{u})^T)) \right] + S_m \quad (2)$$

where p is the pressure, and μ is the dynamic viscosity of the mixture. S_m is the source term of the momentum equation. This term is equal to $(-\frac{\mu \varepsilon^2 \vec{u}}{K})$ for porous mediums and is equal to zero for flow channels, where K is permeability. The conversation of the energy equation is as follows [30]:

$$\nabla \cdot (\rho e C_p \vec{u} T) = \nabla \cdot (k^{eff} \nabla T) + S_Q \quad (3)$$

where T is the temperature, C_p is the specific heat capacity of the mixture, k^{eff} is effective thermal conductivity and S_Q is energy source term which includes the joule heating due to charge transport and heating due to electrochemical reactions. The energy source term for PEMFC and PEMEC are as follows:

$$S_{Q,fc} = j \left(\eta + T \frac{d\varphi_{oc}}{dT} \right) + \sigma_s^{eff} (\nabla \varphi_s)^2 + \sigma_e^{eff} (\nabla \varphi_e)^2 \quad (4)$$

$$S_{Q,el} = j \left(\eta - T \frac{d\varphi_{oc}}{dT} \right) + \sigma_s^{eff} (\nabla \varphi_s)^2 + \sigma_e^{eff} (\nabla \varphi_e)^2 \quad (5)$$

where heat sources η is heat source from the reversible reaction, $T \frac{d\varphi_{oc}}{dT}$ is the entropic heat source due to electrochemical reactions and $\sigma_s^{eff} (\nabla \varphi_s)^2$ and $\sigma_e^{eff} (\nabla \varphi_e)^2$ are ohmic heating. The Maxwell–Stefan equation is used to describe the multispecies mass transports in the whole computational, which solves for the fluxes of each species in terms of the mass fraction. The conversation of species equation is as follows [33,34]:

$$\nabla \cdot [\rho \omega_i \vec{u}] = -\nabla \cdot \left[-\rho \omega_i \sum_{j=1}^N D_{ij} \left[\frac{M}{M_j} \left(\nabla \omega_i + \omega_i \frac{\nabla M}{M} \right) + (x_j - \omega_j) \frac{\nabla p}{p} \right] \right] + R_i \quad (6)$$

where ω_i is the mass fraction of species i , D_{ij} is the binary diffusion coefficient, x is the molar fraction, M is the molecular mass and R_i is the rate expression describing the production of products or consumption of reactants. For PEMFC, the reaction rates in the catalyst layer are as follows [34]:

$$R_{H_2} = -\frac{j_a M_{H_2}}{2F} \quad (7a)$$

$$R_{O_2} = -\frac{j_c M_{O_2}}{4F} \quad (7b)$$

$$R_{H_2O} = \frac{j_c M_{H_2O}}{2F} \quad (7c)$$

where j_a and j_c are current transfer density of anode and cathode, respectively, and F is Faraday constant. For PEMEC, the reaction rates in the catalyst layer are as follows [35]:

$$R_{H_2} = \frac{j_c M_{H_2}}{2F} \quad (8a)$$

$$R_{O_2} = \frac{j_a M_{O_2}}{4F} \quad (8b)$$

$$R_{H_2O} = -\frac{j_a M_{H_2O}}{2F} \quad (8c)$$

The binary diffusivities D_{ij} in Eq. (4), can be calculated as follows [36,37]:

$$D_{ij} = D_{ij0} \varepsilon^{1.5} \left(\frac{T}{T_0} \right)^{1.5} \quad (9)$$

where is T_0 reference temperature and D_{ij0} is reference binary diffusivity.

In the PEMFC and PEMEC, the current can be divided into two parts, ionic and electronic current. Electron transfer occurs in the solid matrix to form an electronic current, and proton transfer through the membrane to create an ionic current. The current conservation equation for solid matrix and membrane are respectively as follows [30,38]:

$$\nabla \cdot (\sigma_s \nabla \varphi_s) + S_s = 0 \quad (10)$$

$$\nabla \cdot (\sigma_m \nabla \varphi_m) + S_m = 0 \quad (11)$$

where σ_s and σ_m are effective electric conductivity of solid matrix and membrane, respectively, and φ is the phase potential. S_s and S_m are the source term of the current conservation equation for matrix and membrane, respectively. The source terms for the catalyst layers of anode and cathode sides of PEMFC are as follows [30]:

$$\text{Anode: } j_s = -j_a, j_m = +j_a \quad (12)$$

$$\text{Cathode: } j_s = +j_c, j_m = -j_c \quad (13)$$

And for PEMEC [6]:

$$\text{Anode: } j_s = +j_a, j_m = -j_a \quad (14)$$

$$\text{Cathode: } j_s = -j_c, j_m = +j_c \quad (15)$$

The source terms in the conversation of species and charge equations are correlated with the current transfer density of anode and cathode. The current transfer densities can be calculated using the Butler–Volmer equation. The Butler–Volmer equation shows the relationship between the current at the interface of the electrode and the electrolyte with the overpotential. For the PEMFC, the current densities of anode and cathode are as follows [39]:

$$j_a = a j_{0,a}^{ref} \left(\frac{C_{H_2}}{C_{H_2,ref}} \right)^{0.5} \left(e^{\frac{a \alpha F}{RT} \eta_a} - e^{-\frac{a \alpha F}{RT} \eta_a} \right) \quad (16)$$

$$j_c = a j_{0,c}^{ref} \left(\frac{C_{O_2}}{C_{O_2,ref}} \right) \left(-e^{\frac{a \alpha F}{RT} \eta_c} + e^{-\frac{a \alpha F}{RT} \eta_c} \right) \quad (17)$$

where $j_{0,a}^{ref}$ is the reference exchange current density per active surface area, a is the specific active surface area (m^{-1}), C and C_{ref} are the local concentration of the species and their reference values, R is the universal gas constant, α is the transfer coefficient, and η is the potential difference between solid matrix and electrolyte, which is the driving force of the transfer of protons and electrons between the solid matrix and electrolyte. η , also called the activation overpotential. For the PEMFC, the activation overpotentials of anode and cathode can be obtained as [34]:

$$\text{Anode: } \eta_a = \varphi_s - \varphi_m \quad (18)$$

$$\text{Cathode: } \eta_c = \varphi_s - \varphi_m - V_{oc} \quad (19)$$

where is open-circuit voltage, and for the PEMEC, the overpotential is as follows [6]:

$$\eta = \varphi_s + \varphi_m + V_{oc} \quad (20)$$

The geometrical dimensions and physical parameters for modeling the PEMFC and PEMEC are listed in Table 1.

3.1.2. Boundary conditions

For the channel inlets of the anode and cathode sides, the values of velocity and mass fractions of H_2 , O_2 , and H_2O are prescribed. It is assumed that the flow in the channels is laminar and for that PEMFC, the inlet fuel, hydrogen, is fully humidified. For both the PEMFC and PEMEC at the outlets of the channels, the boundary is the pressure-outlet. It was set to the atmospheric pressure. For the PEMFC, the anode current collector potential is set to zero, and on the cathode side, the potential is set to the fuel cell voltage. For the PEMEC, The voltage of the current collector is set zero for the cathode side, and the voltage is set to open-circuit voltage for the anode side. All other outside boundaries are set to be insulated with zero flux.

3.2. Analytical model

This study assumes that the PEMFC uses all the produced hydrogen to generate electricity. The efficiency of the PEMEC is defined as the ratio of produced hydrogen to the consumed electrical energy [50]:

$$\eta_{el} = \frac{\dot{n}_{H_2,prod} \bar{HHV}}{P_{el} + \dot{Q}_{el}} \quad (21)$$

where $\dot{n}_{H_2,prod}$ is the amount of produced hydrogen (mol.s^{-1}) and \bar{HHV} is the molar high heat value of hydrogen, P_{el} is the power consumption by the PEMEC and \dot{Q}_{el} is the inlet thermal power input to the PEMEC. The amount of power consumption by the PEMEC is defined as the product of the voltage and the current:

$$P_{el} = V_{el} \cdot I_{el} \quad (22)$$

Furthermore, the inlet thermal energy to the electrolyzer can be calculated as follows:

$$\dot{Q}_{el} = I_{el} \cdot (V_m - V_{el}) \quad (23)$$

where is the thermoneutral voltage of the PEMEC and can be obtained as follows:

$$V_m = 1.485 - 1.49 \cdot 10^{-4} \cdot (T_{el} - 273.15) - 9.84 \cdot 10^{-8} \cdot (T_{el} - 273.15)^2 \quad (24)$$

The amount of produced hydrogen is equal to:

$$\dot{n}_{H_2,prod} = \frac{I_{el}}{2F} \quad (25)$$

where F is the Faraday constant. For a fuel cell, the efficiency is defined as follows [51]:

$$\eta_{fc} = \frac{P_{fc}}{\dot{n}_{H_2,con} \bar{HHV}} \quad (26)$$

where $\dot{n}_{H_2,con}$ is the amount of consumed hydrogen by the fuel cell, which is equal to the amount of produced hydrogen by the electrolysis cell:

$$\dot{n}_{H_2,con} = \frac{I_{fc}}{2F} \quad (27)$$

The amount of generated power by the fuel cell is as follows:

$$P_{fc} = V_{fc} \cdot I_{fc} \quad (28)$$

Table 1
Geometrical and physical operating parameters of the PEMFC and PEMEC.

Parameter	Value
PEM Fuel Cell (PEMFC)	
Channel length, L (m)	0.03
Current collector height, H_{cc} (m)	2×10^{-3} [40]
Current collector width, W_{cc} (m)	2×10^{-3} [40]
Channel height, H_{ch} (m)	1×10^{-3} [40]
Channel width, W_{ch} (m)	1×10^{-3} [40]
Land width, W_{rib} (m)	0.5×10^{-3} [30]
Catalyst layer thickness, t_{cl} (m)	0.02×10^{-3} [30]
GDL thickness, t_{gdl} (m)	0.26×10^{-3} [40]
Membrane thickness, t_m (m)	0.23×10^{-3} [40]
Anode side transfer coefficient, α_a	0.5 [40]
Cathode side transfer coefficient, α_c	1 [40]
Anode ref. exchange current density, $j_{0,a}^{ref}$ ($\text{A} \cdot \text{m}^{-2}$)	6000 [40]
Cathode ref. exchange current density, $j_{0,c}^{ref}$ ($\text{A} \cdot \text{m}^{-2}$)	1.64×10^{-4} [41]
The porosity of GDL, ϵ_{gdl}	0.4 [40]
The porosity of catalyst layer, ϵ_{cl}	0.4
Permeability, K (m^2)	1.8×10^{-18} [40]
Relative humidity of fuel and air sides	100% [40]
The active surface area of whole-cell, $A_{cell,fc}$ (cm^2)	232 [42]
Electrical conductivity of GDL, $\sigma_{s,gdl}$ ($\text{ohm}^{-1} \cdot \text{m}^{-1}$)	5000 [30]
Electrical conductivity of catalyst layer, $\sigma_{s,cl}$ ($\text{ohm}^{-1} \cdot \text{m}^{-1}$)	1000 [30]
Electrical conductivity of membrane, σ_m ($\text{ohm}^{-1} \cdot \text{m}^{-1}$)	6 [40]
Air stoichiometric flow ratio	1
Fuel stoichiometric flow ratio	1
Open circuit voltage, V_{oc} (V)	1 [30]
Operating Temperature, T_{fc} (K)	353
PEM Electrolyzer Cell (PEMEC)	
Channel length, L (m)	0.05 [6]
Current collector height, H_{cc} (m)	2×10^{-3} [40]
Current collector width, W_{cc} (m)	2×10^{-3} [40]
Channel height, H_{ch} (m)	1×10^{-3} [43]
Channel width, W_{ch} (m)	1×10^{-3} [43]
Land width, W_{rib} (m)	0.5×10^{-3} [6]
Catalyst layer thickness, t_{cl} (m)	0.02×10^{-3} [6]
GDL thickness, t_{gdl} (m)	0.20×10^{-3} [43]
Membrane thickness, t_m (m)	0.178×10^{-3} [43]
Anode side transfer coefficient, α_a	2 [44]
Cathode side transfer coefficient, α_c	0.5 [44]
Anode ref. exchange current density, $j_{0,a}^{ref}$ ($\text{A} \cdot \text{cm}^{-2}$)	1×10^{-7} [44,45]
Cathode ref. exchange current density, $j_{0,c}^{ref}$ ($\text{A} \cdot \text{cm}^{-2}$)	1×10^{-3} [44,45]
The porosity of GDL, ϵ_{gdl}	0.3 [43]
The porosity of catalyst layer, ϵ_{cl}	0.3
GDL permeability, K (m^2)	1×10^{-12} [6]
	1.58×10^{-18} [46]

(continued on next page)

Table 1 (continued)

Parameter	Value
Membrane permeability, K (m^2)	
The active surface area of whole-cell, $A_{cell,ec}$ (cm^2)	160 [46]
Electrical conductivity of GDL, σ_{gdl} ($\text{ohm}^{-1} \cdot \text{m}^{-1}$)	5000 [6]
Electrical conductivity of catalyst layer, σ_{cl} ($\text{ohm}^{-1} \cdot \text{m}^{-1}$)	1000 [6]
Electrical conductivity of membrane, σ_m ($\text{ohm}^{-1} \cdot \text{m}^{-1}$)	$(0.005139\lambda - 0.00326)\exp(1268(1/303 - 1/T_{el}))$ [47,48]
Membrane humidification degree, λ	22 [46]
Open circuit voltage, V_{oc} (V)	1.23 [49]
Operating Temperature, T_{el} (K)	353
<i>Other parameters</i>	
Reference diffusivity of H_2 , $D_0^{H_2}$ ($\text{m}^2 \cdot \text{s}^{-1}$)	11×10^{-5} [30]
Reference diffusivity of O_2 , $D_0^{O_2}$ ($\text{m}^2 \cdot \text{s}^{-1}$)	3.2×10^{-5} [30]
Reference diffusivity of H_2O , $D_0^{H_2\text{O}}$ ($\text{m}^2 \cdot \text{s}^{-1}$)	7.35×10^{-5} [30]
Operating pressure, p (atm)	1
Faraday constant, F (C.mol^{-1})	96,485
Universal gas constant, \bar{R} ($\text{J.mol}^{-1} \cdot \text{K}^{-1}$)	8.314

Finally, the efficiency of the combined system of the PEMFC and PEMEC to produce power is defined as the product of the efficiency of the PEMEC and the efficiency of the PEMFC:

$$\eta_{sys} = \eta_{fc} \cdot \eta_{el} \quad (29)$$

In addition to thermodynamic analysis, the system's economic analysis can help design it. The investment cost of PEMFC can be calculated as follows [52,53]:

$$C_{cc,fc} = (C_{st} + C_{BOP})A + C_{asm}P_{fc} \quad (30)$$

where C_{st} is stack cost and C_{BOP} includes the cost of air blowers, humidifiers, radiators, stainless steel pumps, iron pumps, electronic control equipment, starters, and valves, and estimated that it is approximately 34% of the cost of the PEMFC. C_{asm} is the cost of assembly of the PEMFC. C_{st} includes cost of membranes, electrodes, platinum, current collectors, and peripherals [53]:

$$C_{st} = C_{mem} + C_{ele} + C_{bpp} + C_{pt} + C_{phm} \quad (31)$$

The investment cost of the PEMEC is defined as follows [54]:

$$C_{cc,el} = 1000P_{el} \quad (32)$$

In addition, the fuel cost is defined as follows [55]:

$$C_{fuel} = \frac{\dot{m}_{H_2} C_{H_2}}{\eta_{sys,ave}} \quad (33)$$

where \dot{m}_{H_2} is the mass flow rate of the consumed hydrogen, C_{H_2} is the cost of hydrogen per unit mass, and $\eta_{sys,ave}$ is the average efficiency of the system. Also, the cost of maintenance of the fuel cell and electrolysis cell is considered as 5% of the investment cost [7]:

$$C_{O&M} = 0.05C_{cc} \quad (34)$$

All costs in the above equations must be calculated annually to consider the depreciation and time value of money. Using the capital recovery factor (CRF), the annual investment cost will be as follows [56]:

$$C_{cc,an} = \frac{(C_{cc,fc} + C_{cc,el})CRF}{3600} \quad (35)$$

$$CRF = \frac{r \cdot (1+r)^n}{[(1+r)^n - 1]} \quad (36)$$

where r is the interest rate, and n is the system lifetime. Furthermore, for fuel cost [52]:

$$C_{fuel,an} = \sum_{j=1}^n \sum_{t=0}^H \frac{C_{fuel} \cdot t}{(1+r)^n} \quad (37)$$

where H is the annual operating hours of the system. Generated electricity by the PEMFC is calculated annually as a function of load characteristics:

$$W_{prod,an} = \frac{P_{fc} \cdot H \cdot CF}{1000} \quad (38)$$

where CF is the capacity factor. The CF is a ratio that describes the difference between the actual energy produced and the energy produced at full power. The leveledized cost of electricity generation is defined for the system as follows [7]:

$$C_{levelized} = \frac{C_{cc,an} + C_{fuel,an} + C_{O&M}}{W_{prod,an}} \quad (39)$$

The related cost parameters used in the above equations to calculate the leveledized cost of electricity are given in Table 2.

Since the PEMFC and PEMEC were numerically simulated, the voltage-current density curves of the PEMFC and PEMEC were curve fitted for the analytical optimization procedure. The relationships between voltage and current density of the PEMFC and PEMEC are as follows, respectively:

$$V_{fc} = \sum_{i=1}^5 a_i \exp \left[- \left(\frac{i_{fc} - b_i}{c_i} \right)^2 \right], R^2 = 0.999 \quad (40)$$

$$V_{el} = m \cdot i_{el}^n + q, R^2 = 0.999 \quad (41)$$

The fitted constant parameters were obtained for the above Eqs. (40) and (41) are presented in Table 3.

The Eqs. (40) and (41) were used in Eqs. (22) and (28) to calculate the power consumption and power output of the PEMEC and PEMFC, respectively, and related correlations in the 3.2 section.

3.3. Solution methodology

The aforementioned governing equations for the 3-D PEMFC and PEMEC models are solved using the finite element method by commercial software COMSOL Multiphysics. In the finite element method of COMSOL, the electrochemical currents are modelled by the Secondary Current Distribution interface using Ohm's law. This interface was

Table 2
Cost parameters for economic analysis.

Parameter	Value
Nafion membrane 117, C_{mem} ($\text{\$}\cdot\text{m}^{-2}$)	2455.56 [53]
Platinum; 2–4 thickness, C_{pt} ($\text{\$}\cdot\text{m}^{-2}$)	176.29 [53]
Electrode; max. 0.8 mm for single-cell, C_{ele} ($\text{\$}\cdot\text{m}^{-2}$)	177 [55]
Bi-polar plate; max. 4 mm, C_{bpp} ($\text{\$}\cdot\text{m}^{-2}$)	1650 [55]
Peripheral parts, C_{phm} ($\text{\$}\cdot\text{m}^{-2}$)	15.6 [55]
Assembly, C_{asm} ($\text{\$}\cdot\text{kW}^{-1}$)	391 [53]
Interest rate, r	0.185 [56]
Cost of hydrogen, C_{H_2} ($\text{\$}\cdot\text{kg}^{-1}$)	1.00 [52]
System lifetime, n (years)	15 [52]
Annual operating hours, H (hours)	7886 [7]
Capacity factor, CF	0.5

Table 3

The fitted constant parameters for the correlation between voltage and current density of the PEMFC and PEMEC (operating temperature = 353 K).

PEMFC	$i = 1$	$i = 2$	$i = 3$	$i = 4$	$i = 5$
a	1.067e+04	1.152	0.3476	-4.558	3.234
b	-0.7396	-0.2529	0.3118	57.61	0.8998
c	0.2233	0.4498	0.4874	83.63	1.962
PEMFC value					
m	0.8745				
n	0.1517				
q	0.8571				

solved for the GDLs and catalyst layers and the electrolyte membrane. The mass fraction of species and transport through diffusion are which are solved for the flow channels, GDLs, and catalyst layers by using the Transport of Concentrated Species interface and employing the Maxwell-Stefan equations. Transport of Concentrated Species interface coupled with Secondary Current Distribution for the mass sources and sinks. For modeling velocity and pressure the Brinkman equations interface and Navier Stokes equations are employed for the GDLs, catalyst layers, and membrane and the flow channels, respectively. Fig. 3 shows the solution methodology employed in this study. The parameters of Table 1 are used as inputs for the numerical simulation of the PEMFC and PEMEC. The output of the numerical solution curve fitted and the correlations between the voltage and current density of the PEMFC and PEMEC are extracted and then used as input for analytical and economic analysis. The analytical and economic analysis results are employed in the multi-objective optimization procedure.

4. Results and discussion

4.1. Model validation

In order to validate the numerical results of the electrochemical models of the PEMFC and PEMEC, the polarization curves for the PEMFC and PEMEC that are obtained in this study are compared with previous studies. The polarization curve is an essential verification tool for accurately predicting the electrochemical processes of the PEMFC and the PEMEC. The polarization curves were chosen from the experimental results of [41,57] for the electrolyzer and fuel cell, respectively. Furthermore, To ensure the accuracy of the models, the same

geometrical and operating conditions for the PEMFC and PEMEC from these references were applied in modeling. Fig. 4 shows the polarization curves obtained from the present numerical simulation for the PEMFC and PEMEC and those from these references. As shown from Fig. 4, for both the PEMFC and PEMEC, there is a good agreement between the numerical model results and references data at low and medium current densities. At high current densities, numerical modeling results demonstrate smaller quantities and more deviation from the experimental data. This deviation is due to increased generated ohmic heat at higher current densities. It increases the source term of electrical potential in the energy equation that causes more deviation. The results of these models have a deviation of less than 5% for both cases of the PEMEC and PEMFC.

4.2. Performance analysis of integrated system

The effects of temperature on the performance of the PEMEC are shown in Fig. 5. As can be seen, at the higher temperature, the rate of hydrogen production by the PEMEC increases. The kinetics of the charge transfer reaction at the interface between the electrode and the electrolyte improves at higher temperatures. Therefore, the activation overpotential decreases at a higher temperature. Moreover, the ion conductivity increases at higher temperatures, and the concentration overpotential decreases due to the faster kinetics of the reactions. The effects of temperature on the performance of the PEMFC are shown in Fig. 6. It assumed that the PEMFC is a counter-flow fuel cell. As can be observed, the consumption of hydrogen and oxygen increases with an increase in temperature; as a result, fewer hydrogen outflows from the cell. Thus, at the same voltage level, the output current density by the PEMFC increases at higher temperatures which are shown in Fig. 7.

Fig. 7 shows the current density at the membrane of the PEMFC at two different temperatures. As can be seen, due to a decrease in the reactant concentrations, the current density decreases towards the outlets of the PEMFC. Moreover, by comparing Fig. 7(a)–(b), it is clear that at a higher temperature of the PEMEC, the amount of output current density by the PEMFC increases. Therefore, as can be seen, a higher operating temperature of the PEMFC can directly increase the activity of the catalysts and boost the rate of electrochemical reactions.

Fig. 8(a) shows the efficiency and the output power of the integrated PEMFC and PEMEC system with the PEMEC current density at different operating temperatures. As can be seen, the efficiency and output power

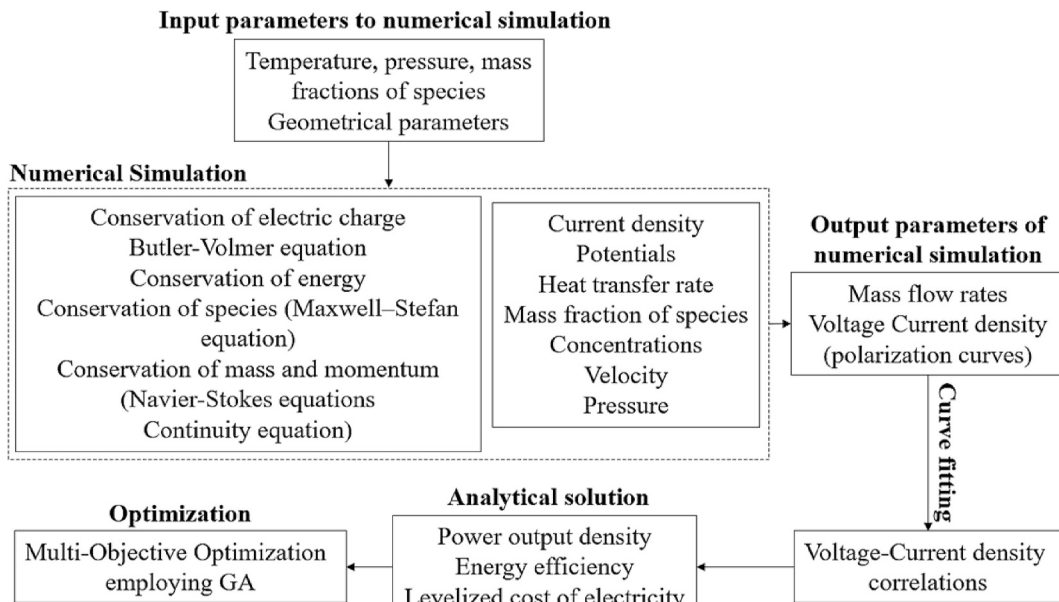


Fig. 3. Solution methodology for analysis of the integrated system.

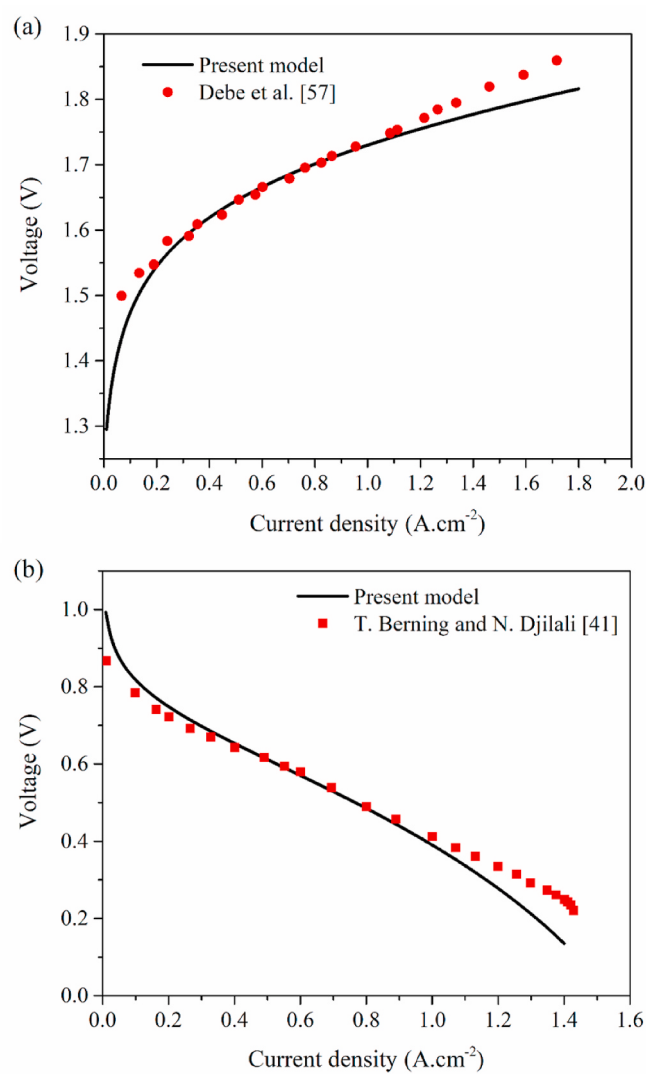


Fig. 4. Comparison of polarization curve between the numerical model of (a) PEMEC and (b) PEMFC with references data [41,57].

of the system have both increased with increasing temperature. Also, the cell's output power reaches a maximum value at a specific current density value and then decreases. At current densities below this value, the behavior of output power and system efficiency are reversed. Where the output power reaches a maximum, the system efficiency has its lowest value.

Furthermore, Fig. 8(b) shows the leveled cost and the output power of the integrated PEMFC and PEMEC system with current density at different operating temperatures. As can be seen, the system's leveled cost decreases with increasing the operating temperature. Furthermore, as the output power of the system increases, the leveled cost of the system increases. Thus, it is desirable to reduce cost and, at the same time, increase the output power of the system. In addition, changing the temperature makes the current density when the power output density reaches its maximum value. Also, as shown in Fig. 8(a), the system's efficiency decreases with increasing the output power, making it difficult to choose between maximum power and maximum efficiency. Therefore, finding the optimal points with optimal output power, efficiency, and the cost is a matter of finding the optimal points.

Fig. 9(a) and (b) shows the effect of the operating pressure of the integrated system on the power output density, efficiency, and leveled cost. Fig. 9(a) shows that the efficiency and output power of the system increases with increasing temperature. Also, the cell's output power

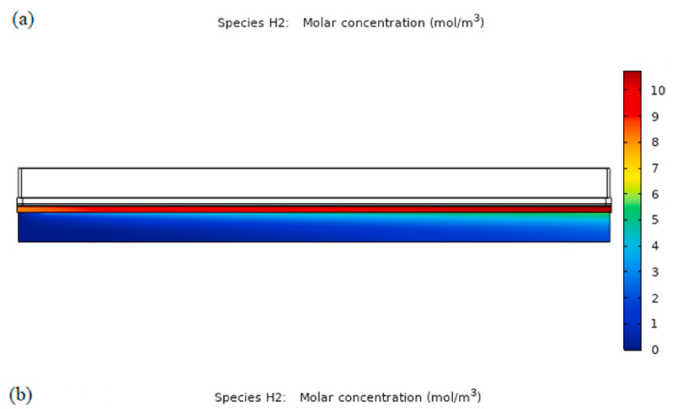


Fig. 5. The PEMEC hydrogen molar concentration at different temperatures, (a) 40 °C and (b) 80 °C.

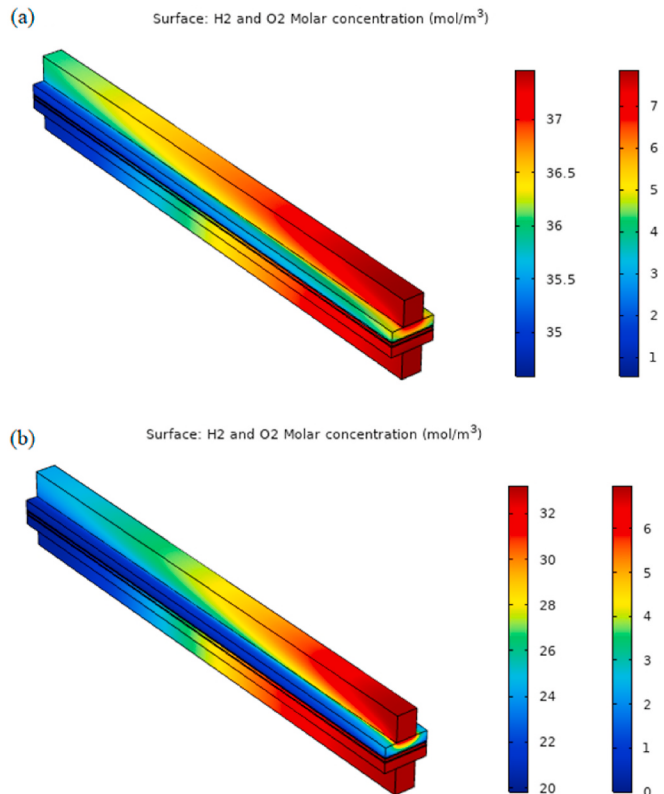


Fig. 6. The PEMFC hydrogen and oxygen molar concentrations at different temperatures, (a) 40 °C and (b) 80 °C.

reaches a maximum value at a specific current density value and then decreases. Furthermore, as shown in Fig. 9(b), the system's leveled cost decreases with increasing the operating pressure. Thus, from Figs. 8

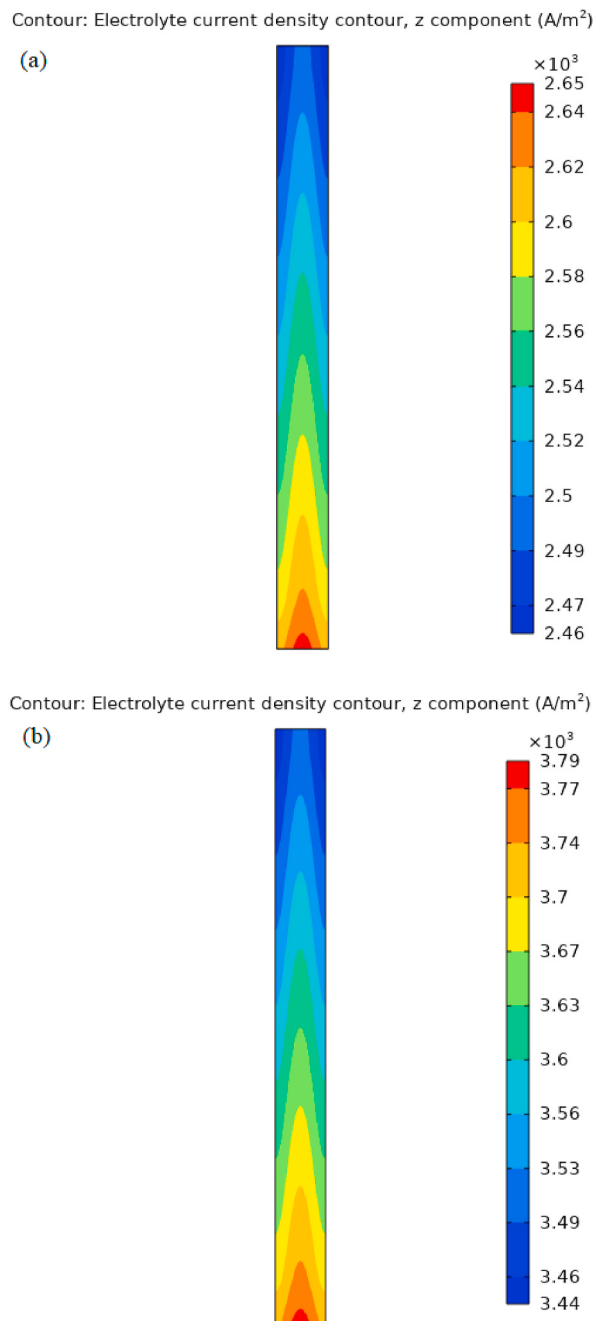


Fig. 7. The current density of the PEMFC at different temperatures, (a) 40 °C and (b) 80 °C.

and 9, it is evident that higher operating temperature and pressure cause higher power output and efficiency and lower leveled cost of the integrated system.

4.3. Optimization of the integrated system

According to the results obtained from Figs. 8(a) and 9(a), the integrated system's power output density and efficiency behave in reverse. Therefore, the necessity of using multi-objective optimization to find the optimal power output density and efficiency of the integrated system is obvious. Furthermore, according to Figs. 8(b) and 9(b), the system's leveled cost increases with increasing the current density. The power output density of the integrated system increases and reaches a maximum value, and then decreases. Thus, three scenarios for

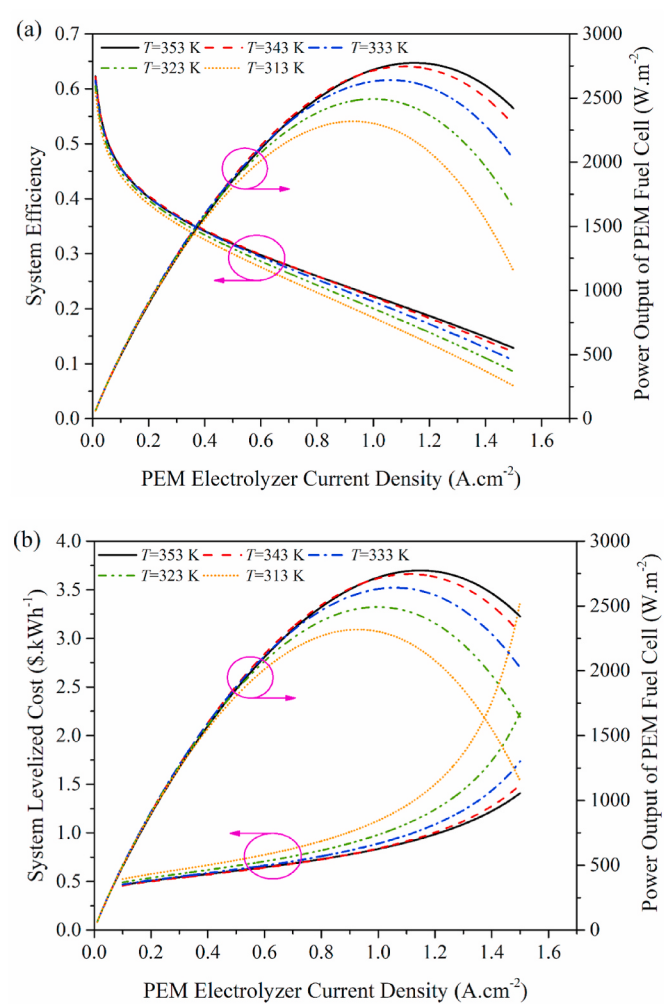


Fig. 8. (a) The efficiency and output power of the integrated system for power generation with the PEMEC current density, (b) The leveled cost and output power of the integrated system for power generation with the PEMEC current density.

optimizing the integrated system are considered in the following. For the first scenario, power output density and energy efficiency are considered objective functions for maximization. Then in the second scenario, Power output density and leveled cost are considered, which have to be maximized and minimized, respectively. Finally, the third objective functions for the third scenario are power output density and energy efficiency, which must be maximized, with leveled cost, which must be minimized.

A multi-objective process includes simultaneous minimizing or maximizing many objectives, with a number of inequality or equality constraints. The genetic algorithm (GA) technique is applied to optimize the objective functions in many studies [58–60]. GAs are semi-stochastic techniques inspired by natural selection. The first multi-objective GA was presented by Schaffer [61] and called vector evaluated GA (VEGA). An algorithm developed by Srinivas and Deb [62] based on non-dominated sorting, which was called the non-dominated sorting genetic algorithm (NSGA). Deb et al. later modified [63] the NSGA by omitting higher computational complications, lack of elitism, and the requirement for defining the sharing parameter, which is called the non-dominated sorting genetic algorithm II (NSGA-II). A solution for multi-objective optimizations is to evaluate a series of solutions that satisfy the objectives within an allowable level without being dominated by other solutions. These solutions are called Pareto optimal Frontiers (POFs). This method was entirely described in Ref. [60]. In this study,

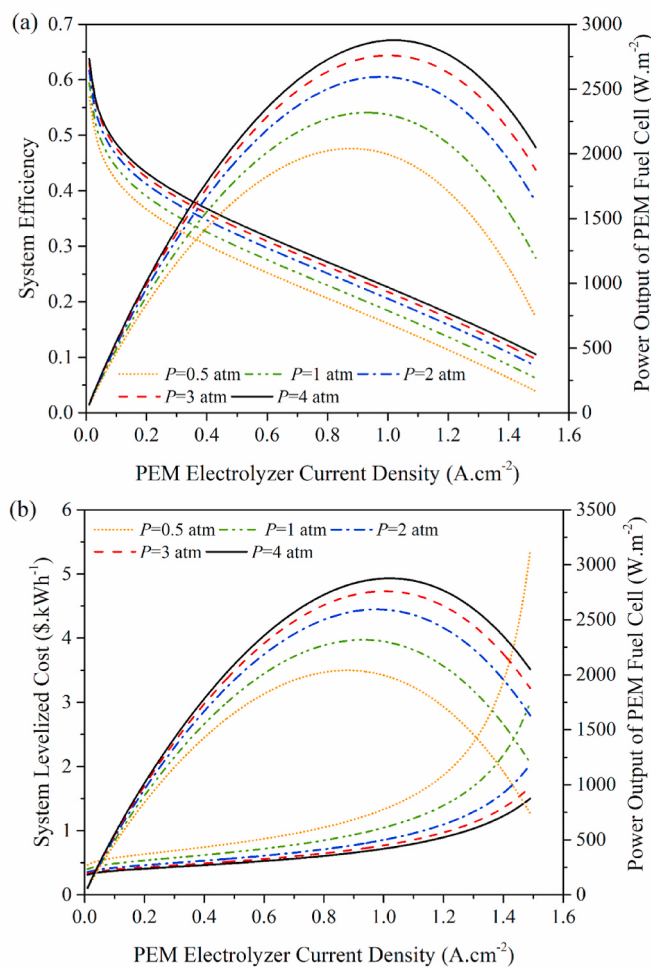


Fig. 9. (a) The efficiency and output power of the integrated system for power generation with the PEMEC current density at different pressures, (b) The efficiency and output power of the integrated system for power generation with the PEMEC current density at different pressures.

NSGA-II has been employed for finding POFs. In multi-objective optimization, decision-making is needed to find the best optimal solution among POFs solutions. In this paper, three decision-making tools include, LINMAP, TOPSIS, and fuzzy Bellman-Zadeh employed to select the final optimal solution. Details of these decision-making methods were entirely described in Ref. [64].

The Pareto optimal frontier for the first scenario was depicted in Fig. 10. Also, the final optimal solution was selected using three decision-making, and selected points were shown in Fig. 10. In Fig. 10, points A and B, respectively, represent the state in which the energy efficiency and power output density are considered as objective functions for single-objective optimization. The ideal point indicates the most desirable state in which both objective functions are at their maximum value, and the non-ideal point indicates the state in which the two objective functions are at their lowest. Specifications of the final optimal solution recommended by the LINMAP, TOPSIS, and fuzzy decision-makers for the first scenario are indicated in Table 4. Table 4 shows that the TOPSIS decision-making method presents a higher value for power output density compared to other decision-making techniques; therefore, it seems that in this case, TOPSIS provides a more desirable final optimal solution. The optimal solution values obtained by TOPSIS for power output density and efficiency are about 92% and 55.1% of the ideal point values, respectively.

In the second scenario, power output density with leveled cost is considered the objective function. Fig. 11 represents the Pareto frontier

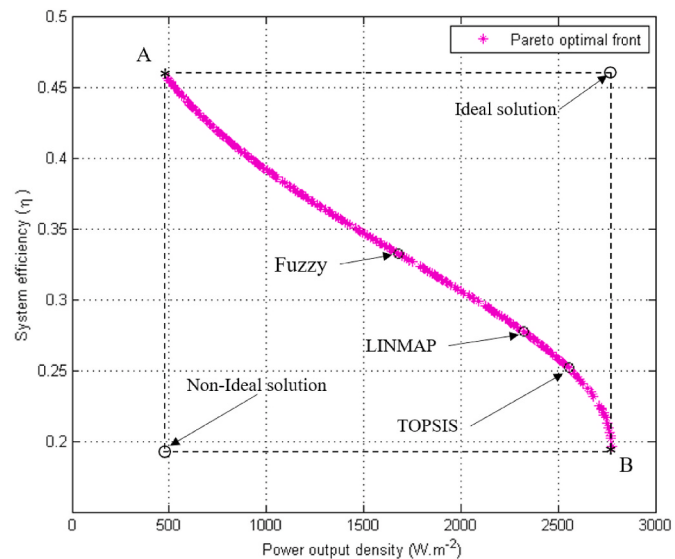


Fig. 10. Pareto optimal frontier curve of the first scenario.

Table 4
Outcomes of the decision-makers for the first scenario.

Decision-making method	Decision variable	Considered objective functions	
		i_{el} (A.cm^{-2})	P_{fc} (W.m^{-2})
TOPSIS	0.841	2552.97	0.252
LINMAP	0.702	2321.25	0.278
Fuzzy	0.436	1679.85	0.333
Ideal point	—	2774.01	0.457
Non-ideal point	—	490.78	0.197

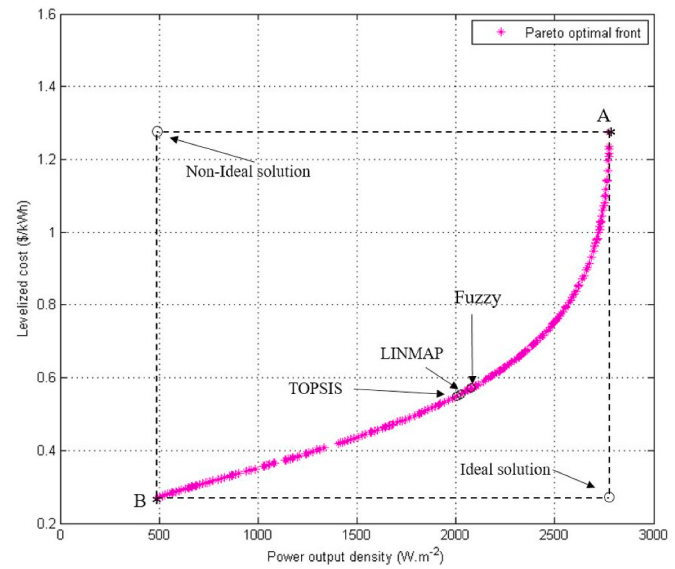


Fig. 11. Pareto optimal frontier curve of the second scenario.

curve achieved in the second optimization scenario. Specifications of the final optimal solution recommended by the LINMAP, TOPSIS, and fuzzy decision-makers for the second scenario are indicated in Table 5. Considering the ideal and non-ideal points of these two objective functions together, especially the system's leveled cost, it seems that in this case, the TOPSIS decision-maker method gives a more desirable final optimal solution. The optimal solution value obtained by TOPSIS for power output density is about 92% of the ideal point value, and the

Table 5

Outcomes of the decision-makers for the second scenario.

Decision-making method	Decision variable	Considered objective functions	
		i_{el} (A.cm $^{-2}$)	P_{fc} (W.m $^{-2}$)
TOPSIS	0.669	2002.25	0.549
LINMAP	0.702	2023.87	0.555
Fuzzy	0.901	2079.19	0.571
Ideal point	—	2774.02	0.270
Non-ideal point	—	490.32	1.274

value of leveled cost is about 43.1% lower than that of the non-ideal point value.

According to the results obtained from Figs. 8 and 9 together as well as the behavior of power output density, efficiency, and cost of the integrated system, these three variables are considered objective functions for the third scenario. The ultimate aim of the optimization is to maximize the output power and efficiency and minimize the system's leveled cost. The current density of the PEMEC is considered a decision variable. In fact, by finding the optimum current density of the PEMEC, the optimum amount of hydrogen production and consumption will be determined according to Eqs. (25) and (27). The multi-objective optimization's three-dimensional Pareto optimal frontier surface was demonstrated in Fig. 12. Also, the best final optimal solution was chosen by applying three decision-making, and selected points were shown in Table 6. Specifications of the final optimal solution suggested by the TOPSIS, LINMAP, and fuzzy decision techniques are presented in Table 6. Table 6 reveals that the TOPSIS decision-making method presents a lower value for the system's leveled cost than other decision-making methods. Compared to the Fuzzy decision-making method, the leveled cost is about 6% higher; however, the power out density is about 8% higher; hence, in this case, it seems that TOPSIS provides a more favorable final optimal solution. The obtained leveled cost of the integrated system demonstrate that the selling price of electricity is not competitive with the average industrial selling price in the US, which is about 0.05–0.2 \$.kWh $^{-1}$; however, it is comparable to non-conventional energy systems in rural regions, which is about 0.25–0.3 \$.kWh $^{-1}$ [8]. However, the costs of PEMFCs and PEMECs are expected to significantly improve over time, according to road maps and research [65]. Furthermore, the optimum current density of the PEMEC is 0.479 A.cm $^{-2}$.

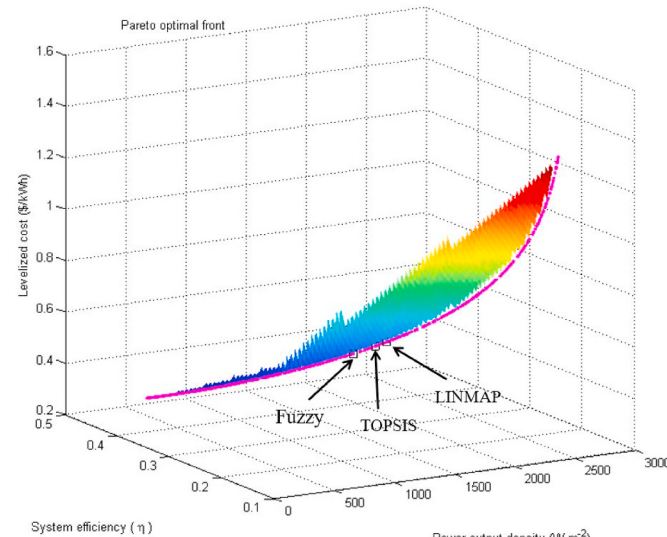


Fig. 12. Pareto optimal frontier surface for the objective functions of the third scenario.

Table 6

Outcomes of the decision-makers for the third scenario.

Decision-making method	Decision variable	Considered objective functions		
		i_{el} (A.cm $^{-2}$)	P_{fc} (W.m $^{-2}$)	η_{sys}
TOPSIS	0.479	1801.87	0.323	0.498
LINMAP	0.506	1874.33	0.317	0.516
Fuzzy	0.432	1669.20	0.333	0.469

5. Conclusions

The combination of the PEMFC and PEMEC for power generation was investigated in this paper. For this purpose, the three-dimensional model of the PEMFC and PEMEC were numerically simulated. In this regard, the PEMFC and PEMEC were integrated as power generation systems. Due to the intermittent nature of renewable energy technologies and the need to increase the security of electricity supply with these technologies, the purpose of the integrated system is influenced by these two factors. Due to the intermittent nature of renewable energy technologies and the need to increase the security of electricity supply with these technologies, the purpose of the integrated system was influenced by these two factors. PEMEC can use the excess electricity generated by renewable energy technologies to produce hydrogen. At the peak of demand, this hydrogen can be used by PEMFC to generate power. Results showed that as the current density of the PEMEC increases, the output power of the combined system increases and reaches a maximum, and then decreases. However, the efficiency of the combined system decreased with increasing the current density of the PEMEC. Also, both the output power and efficiency increased with increasing the operating temperature of the combined system. Economic analysis was also employed to better design the PEMFC-PEMEC power generation system, and the system's leveled cost of electricity was considered. Results revealed that the system's leveled cost increases as the system's output power increase.

Therefore, a multi-objective optimization was performed, as the aim was to minimize the system's leveled cost and maximize the output power and efficiency of the system simultaneously. The current density of the PEMEC was considered a decision variable. Three decision-making techniques, including LINMAP, TOPSIS, and fuzzy Bellman-Zadeh, were applied to find the final optimal solution among optimal solutions. Outcomes of decision-making techniques showed that TOPSIS provided a more favorable final optimal solution with the lowest value for the leveled cost of the system, 0.498 \$.kWh $^{-1}$, while the efficiency and output power of the combined system were 0.323 and 1801.87 W m $^{-2}$, respectively. In the case of a combined power generation system, this study does not consider hydrogen storage because it assumes that all of the hydrogen produced by the PEMEC is used to generate electricity in PEMFC. In this regard, the main focus was on the performance analysis that employs the green power (power by wind or other renewable energy technologies) to green fuel (hydrogen) in the PEMEC to generate zero-emission electricity by the PEMFC. However, a thorough characterization of hydrogen storage will be necessary to offer a more comprehensive view of this system in future research.

Author statement

Armin Abdollahipour: Conceptualization, Methodology, Software, Investigation, Writing - Review & Editing, Visualization, and Preparing the Revision. **Hoesyn Sayyaadi:** Conceptualization, Methodology, Investigation, Review & Editing as well as Supervision.

Declaration of competing interest

The authors declare that they have no known competing financial interests or personal relationships that could have appeared to influence

the work reported in this paper.

References

- [1] Afshari E, Mosharaf-Dehkordi M, Rajabian H. An investigation of the PEM fuel cells performance with partially restricted cathode flow channels and metal foam as a flow distributor. *Energy* 2017;118:705–15.
- [2] Atyabi SA, Afshari E, Wongwises S, Yan W-M, Hadjadj A, Shadloo MS. Effects of assembly pressure on PEM fuel cell performance by taking into accounts electrical and thermal contact resistances. *Energy* 2019;179:490–501.
- [3] Chavan SL, Talange DB. Modeling and performance evaluation of PEM fuel cell by controlling its input parameters. *Energy* 2017;138:437–45.
- [4] Grigoriev S, Kalinnikov A. Mathematical modeling and experimental study of the performance of PEM water electrolysis cell with different loadings of platinum metals in electrocatalytic layers. *Int J Hydrogen Energy* 2017;42(3):1590–7.
- [5] Marshall A, Borresen B, Hagen G, Tsyplkin M, Tunold R. Hydrogen production by advanced proton exchange membrane (PEM) water electrolyzers—reduced energy consumption by improved electrocatalysis. *Energy* 2007;32(4):431–6.
- [6] Toghiani S, Afshari E, Baniasadi E, Atyabi S, Naterer G. Thermal and electrochemical performance assessment of a high temperature PEM electrolyzer. *Energy* 2018;152:237–46.
- [7] Rahimi S, Meratizaman M, Monadizadeh S, Amidpour M. Techno-economic analysis of wind turbine-PEM (polymer electrolyte membrane) fuel cell hybrid system in standalone area. *Energy* 2014;67:381–96.
- [8] Mohammadi A, Mehrpooya M. A comprehensive review on coupling different types of electrolyzer to renewable energy sources. *Energy* 2018;158:632–55.
- [9] Abdollahipour A, Sayyaadi H. A novel electrochemical refrigeration system based on the combined proton exchange membrane fuel cell-electrolyzer. *Appl Energy* 2022;316:119058.
- [10] Ngoh SK, Njomo D. An overview of hydrogen gas production from solar energy. *Renew Sustain Energy Rev* 2012;16(9):6782–92.
- [11] Alavi O, Mostafaeipour A, Qolipour M. Analysis of hydrogen production from wind energy in the southeast of Iran. *Int J Hydrogen Energy* 2016;41(34):15158–71.
- [12] Mostafaeipour A, Dehshiri SJH, Dehshiri SSH. Ranking locations for producing hydrogen using geothermal energy in Afghanistan. *Int J Hydrogen Energy* 2020;45(32):15924–40.
- [13] Touili S, Merrouni AA, Azouzoute A, El Hassouani Y, Amrani A-i. A technical and economical assessment of hydrogen production potential from solar energy in Morocco. *Int J Hydrogen Energy* 2018;43(51):22777–96.
- [14] Mostafaeipour A, Rezayat H, Rezaei M. A thorough investigation of solar-powered hydrogen potential and accurate location planning for big cities: a case study. *Int J Hydrogen Energy* 2020;45(56):31599–611.
- [15] Khelfaoui N, Djafour A, Ghenai C, Laib I, Danoune M, Gougui A. Experimental investigation of solar hydrogen production PV/PEM electrolyser performance in the Algerian Sahara regions. *Int J Hydrogen Energy* 2021;46(59):30524–38.
- [16] Ayodele T, Munda J. Potential and economic viability of green hydrogen production by water electrolysis using wind energy resources in South Africa. *Int J Hydrogen Energy* 2019;44(33):17669–87.
- [17] Ishaq H, Dincer I, Naterer GF. Performance investigation of an integrated wind energy system for co-generation of power and hydrogen. *Int J Hydrogen Energy* 2018;43(19):9153–64.
- [18] Li Z, Guo P, Han R, Sun H. Current status and development trend of wind power generation-based hydrogen production technology. *Energy Explor Exploit* 2019;37(1):5–25.
- [19] Rezaei M, Mostafaeipour A, Qolipour M, Momeni M. Energy supply for water electrolysis systems using wind and solar energy to produce hydrogen: a case study of Iran. *Front Energy* 2019;13(3):539–50.
- [20] Al-Sharafi A, Sahin AZ, Ayar T, Yilbas BS. Techno-economic analysis and optimization of solar and wind energy systems for power generation and hydrogen production in Saudi Arabia. *Renew Sustain Energy Rev* 2017;69:33–49.
- [21] Rad MAV, Ghasempour R, Rahdan P, Mousavi S, Arastouinia M. Techno-economic analysis of a hybrid power system based on the cost-effective hydrogen production method for rural electrification, a case study in Iran. *Energy* 2020;190:116421.
- [22] Wu W, Christiana VI, Chen S-A, Hwang J-J. Design and techno-economic optimization of a stand-alone PV (photovoltaic)/FC (fuel cell)/battery hybrid power system connected to a wastewater-to-hydrogen processor. *Energy* 2015;84:462–72.
- [23] Dehshiri SSH. A new application of multi criteria decision making in energy technology in traditional buildings: a case study of Isfahan. *Energy* 2022;240:122814.
- [24] Yilmaz C, Kanoglu M. Thermodynamic evaluation of geothermal energy powered hydrogen production by PEM water electrolysis. *Energy* 2014;69:592–602.
- [25] Fan J-L, Yu P, Li K, Xu M, Zhang X. A leveled cost of hydrogen (LCOH) comparison of coal-to-hydrogen with CCS and water electrolysis powered by renewable energy in China. *Energy* 2022;242:123003.
- [26] Seyedmatin P, Karimian S, Rostamzadeh H, Amidpour M. Electricity and hydrogen co-production via scramjet multi-expansion open cooling cycle coupled with a PEM electrolyzer. *Energy* 2020;199:117364.
- [27] Yazdi MZ, Kalbasi M. A novel analytical analysis of PEM fuel cell. *Energy Convers Manag* 2010;51(2):241–6.
- [28] Kerkoub Y, Benzaoui A, Haddad F, Ziari YK. Channel to rib width ratio influence with various flow field designs on performance of PEM fuel cell. *Energy Convers Manag* 2018;174:260–75.
- [29] Moein-Jahromi M, Kermani M. Three-dimensional multiphase simulation and multi-objective optimization of PEM fuel cells degradation under automotive cyclic loads. *Energy Convers Manag* 2021;231:113837.
- [30] Yuan W, Tang Y, Pan M, Li Z, Tang B. Model prediction of effects of operating parameters on proton exchange membrane fuel cell performance. *Renew Energy* 2010;35(3):656–66.
- [31] Nield DA, Bejan A. *Convection in porous media*. Springer; 2006.
- [32] Le Bars M, Worster MG. Interfacial conditions between a pure fluid and a porous medium: implications for binary alloy solidification. *J Fluid Mech* 2006;550:149–73.
- [33] Bird RB, WE Stewart and EN Lightfoot, "Transport Phenomena", second ed. John Wiley & Sons, Inc.; 2002.
- [34] Ubong E, Shi Z, Wang X. Three-dimensional modeling and experimental study of a high temperature PBI-based PEM fuel cell. *J Electrochim Soc* 2009;156(10):B1276.
- [35] Ruiz DDH, Sasmito AP, Shamim T. Numerical investigation of the high temperature PEM electrolyzer: effect of flow channel configurations. *ECS Trans* 2013;58(2):99.
- [36] Um S, Wang CY, Chen K. Computational fluid dynamics modeling of proton exchange membrane fuel cells. *J Electrochim Soc* 2000;147(12):4485.
- [37] Afshari S, Jazayeri S. Effects of the cell thermal behavior and water phase change on a proton exchange membrane fuel cell performance. *Energy Convers Manag* 2010;51(4):655–62.
- [38] Rahgoshay S, Ranjbar A, Ramiar A, Alizadeh E. Thermal investigation of a PEM fuel cell with cooling flow field. *Energy* 2017;134:61–73.
- [39] Mann R, Amphlett J, Peppley B, Thurgood C. Application of Butler–Volmer equations in the modelling of activation polarization for PEM fuel cells. *J Power Sources* 2006;161(2):775–81.
- [40] Berning T, Lu D, Djilali N. Three-dimensional computational analysis of transport phenomena in a PEM fuel cell. *J Power Sources* 2002;106(1–2):284–94.
- [41] Berning T, Djilali N. Three-dimensional computational analysis of transport phenomena in a PEM fuel cell—a parametric study. *J Power Sources* 2003;124(2):440–52.
- [42] Zhao P, Wang J, Gao L, Dai Y. Parametric analysis of a hybrid power system using organic Rankine cycle to recover waste heat from proton exchange membrane fuel cell. *Int J Hydrogen Energy* 2012;37(4):3382–91.
- [43] Han B, Steen III SM, Mo J, Zhang F-Y. Electrochemical performance modeling of a proton exchange membrane electrolyzer cell for hydrogen energy. *Int J Hydrogen Energy* 2015;40(22):7006–16.
- [44] Marangio F, Santarelli M, Cali M. Theoretical model and experimental analysis of a high pressure PEM water electrolyser for hydrogen production. *Int J Hydrogen Energy* 2009;34(3):1143–58.
- [45] García-Valverde R, Espinosa N, Urbina A. Simple PEM water electrolyser model and experimental validation. *Int J Hydrogen Energy* 2012;37(2):1927–38.
- [46] Abdin Z, Webb C, Gray EM. Modelling and simulation of a proton exchange membrane (PEM) electrolyser cell. *Int J Hydrogen Energy* 2015;40(39):13243–57.
- [47] Santarelli M, Torchio M. Experimental analysis of the effects of the operating variables on the performance of a single PEMFC. *Energy Convers Manag* 2007;48(1):40–51.
- [48] Springer TE, Zawodzinski T, Gottesfeld S. Polymer electrolyte fuel cell model. *J Electrochim Soc* 1991;138(8):2334.
- [49] Toghiani S, Afshari E, Baniasadi E. Three-dimensional computational fluid dynamics modeling of proton exchange membrane electrolyzer with new flow field pattern. *J Therm Anal Calorim* 2019;135(3):1911–9.
- [50] Nachi FM, Baniasadi E, Afshari E, Javani N. Performance assessment of a solar hydrogen and electricity production plant using high temperature PEM electrolyzer and energy storage. *Int J Hydrogen Energy* 2018;43(11):5820–31.
- [51] Sohani A, Naderi S, Torabi F. Comprehensive comparative evaluation of different possible optimization scenarios for a polymer electrolyte membrane fuel cell. *Energy Convers Manag* 2019;191:247–60.
- [52] Sohani A, Naderi S, Torabi F, Sayyaadi H, Akhlaghi YG, Zhao X, et al. Application based multi-objective performance optimization of a proton exchange membrane fuel cell. *J Clean Prod* 2020;252:119567.
- [53] Tahmasbi AA, Hoseini A, Roshandel R. A new approach to multi-objective optimisation method in PEM fuel cell. *Int J Sustain Energy* 2015;34(5):283–97.
- [54] Genç G, Çelik M, Genç MS. Cost analysis of wind-electrolyzer-fuel cell system for energy demand in Pınarbaşı-Kayseri. *Int J Hydrogen Energy* 2012;37(17):12158–66.
- [55] Na W, Gou B. The efficient and economic design of PEM fuel cell systems by multi-objective optimization. *J Power Sources* 2007;166(2):411–8.
- [56] Tahmasebzadehbaie M, Sayyaadi H. Efficiency enhancement and NOx emission reduction of a turbo-compressor gas engine by mass and heat recirculations of flue gases. *Appl Therm Eng* 2016;99:661–71.
- [57] Debe M, Hendricks S, Vernstrom G, Meyers M, Brostrom M, Stephens M, et al. Initial performance and durability of ultra-low loaded NSTF electrodes for PEM electrolyzers. *J Electrochim Soc* 2012;159(6):K165.
- [58] Sayyaadi H, Esmaeilzadeh H. Determination of optimal operating conditions for a polymer electrolyte membrane fuel cell stack: optimal operating condition based on multiple criteria. *Int J Energy Res* 2013;37(14):1872–88.
- [59] Abdollahipour A, Sayyaadi H. Thermal energy recovery of molten carbonate fuel cells by thermally regenerative electrochemical cycles. *Energy* 2021;227:120489.
- [60] Sayyaadi H, Aminian HR. Design and optimization of a non-TEMA type tubular recuperative heat exchanger used in a regenerative gas turbine cycle. *Energy* 2010;35(4):1647–57.
- [61] Schaffer JD. Multiple objective optimization with vector evaluated genetic algorithms. Conference Multiple objective optimization with vector evaluated genetic algorithms. Lawrence Erlbaum Associates, Inc., Publishers.

- [62] Srinivas N, Deb K. Multiobjective optimization using nondominated sorting in genetic algorithms. *Evol Comput* 1994;2(3):221–48.
- [63] Deb K, Pratap A, Agarwal S, Meyarivan T. A fast and elitist multiobjective genetic algorithm: NSGA-II. *IEEE Trans Evol Comput* 2002;6(2):182–97.
- [64] Sayyaadi H, Mehrabipour R. Efficiency enhancement of a gas turbine cycle using an optimized tubular recuperative heat exchanger. *Energy* 2012;38(1):362–75.
- [65] International Energy Agency. The future of hydrogen. Jun. 2019.